

Classical noise and flux: the limits of multi-state atom lasers

N. P. Robins, C. M. Savage, J. J. Hope, J. E. Lye, C. S. Fletcher, S. A. Haine, and J. D. Close
Australian Centre for Quantum Atom Optics, The Australian National University, Canberra, 0200, Australia.

By direct comparison between experiment and theory, we show how the classical noise on a multi-state atom laser beam increases with increasing flux. The trade off between classical noise and flux is an important consideration in precision interferometric measurement. We use periodic 10 s radio-frequency pulses to couple atoms out of an $F = 2$ ^{87}Rb Bose-Einstein condensate. The resulting atom laser beam has surprising structure which is explained using three dimensional simulations of the ve state Gross-Pitaevskii equations.

PACS numbers: 03.75.Pp, 03.75.Mn

It is the high flux, spectral density, and associated first order coherence that has made the optical laser central to many technologies. In the field of precision measurement, atom lasers hold similar promise [1]. In a Sagnac interferometer, for example, the inherent sensitivity of a matter wave gyroscope exceeds that of a photon gyroscope with the same particle flux and area by 11 orders of magnitude [2]. In any practical application of interferometry to high precision measurement, whether it be with photons or atoms, there will be a trade off between the classical noise and the quantum noise or flux of the source. In this Letter, we investigate this trade off for an atom laser.

In an unpumped laser, classical noise is the presence of unwanted excited dynamical modes. We find agreement between our experimental results and a full 3D Gross-Pitaevskii (GP) model, and show that at high flux, classical noise increases with increasing flux. That we can achieve agreement between a 3D theory including all Zeeman states and experiment is significant. It is highly likely that the much sought-after pumped atom laser will operate under rather specific conditions of scattering length, temperature and number density [3], and experiments will need to be guided by accurate theoretical models that must be validated against experiments if we are to trust their detailed predictions.

Mewes et al. [4] demonstrated the first atom laser based on the application of pulsed radio-frequency (RF) fields to induce controlled spin flips from magnetically trapped to un-trapped states of a Bose-Einstein condensate. Later it was shown by Hagley et al. that a pulsed Raman out-coupling could be used to achieve a quasi-continuous multi-state atomic beam [5]. Bloch et al. achieved continuous RF out-coupling for up to 100 ms, producing a single state atom laser beam, and showed that this beam could be coherently manipulated in direct analogy to the optical laser [6, 7]. Both temporal and spatial coherence have been measured, and it has been demonstrated that RF outcoupling preserves the coherence of the condensate [8, 9, 10]. The beam divergence has been measured [11], and there has been one real time measurement of the flux of an atom laser beam

[12]. Ballagh et al. [13] introduced the Gross-Pitaevskii equation as an effective tool for investigating the atom laser within the semi-classical mean-field approximation and a number of groups found good agreement between GP models and experiment [14, 15]. Rabi cycling between Zeeman components, a manifestation of the non-Markovian nature of the atom laser [16, 17], was observed in the experiment of Mewes et al. and could be expected to significantly increase the amplitude, and possibly frequency, noise of the beam. There has been no investigation of the relationship between classical noise and flux in an atom laser, and it is this aspect that we investigate both experimentally and theoretically in this Letter.

Experimentally, a continuous atom laser based on resonant output coupling puts stringent limits on the stability of cold atom traps [6]. Typical condensates have a resonant width of 10 kHz. Output coupling requires a stable magnetic bias, B_0 , at the 0.1 mG level, one to two orders of magnitude better than typical magnetic traps. In comparison, a pulsed atom laser is relatively straightforward to implement. A 10 s pulse has a frequency width of 200 kHz, significantly broader than both the 10 kHz resonant width of the condensate, and the instability of our trap which fluctuates within the range 15 kHz due mainly to thermal fluctuations of the coils. In the work reported in this Letter, we have opted to study a pulsed atom laser to ensure shot to shot reproducibility and allow detailed quantitative comparison to numerical models. We have chosen to study atom laser beams derived from an $F = 2; m_F = 2$ condensate because of the richness and complexity offered by the system, although non-Markovian effects are present even in two-component atom lasers due to the nonlinear atomic dispersion relations.

In our experiment, we produce an $F = 2; m_F = 2$ ^{87}Rb condensate, consisting of approximately 50,000 atoms, via evaporation in a water-cooled QUIC magnetic trap [18] with a radial trapping frequency $\nu_r = 253$ Hz, an axial trapping frequency $\nu_z = 20$ Hz, and a bias field $B_0 = 1$ G. After evaporative cooling, the BEC was left to equilibrate for 100 ms. We then triggered an RF signal generator set in gated burst mode. The RF pulses

were amplified (35 dB) and radiated perpendicular to the magnetic bias field of the trap through a 22 mm radius single loop, approximately 18 mm from the BEC. To ensure that we had calibrated all experimental parameters correctly, we made an initial series of measurements of the number of trapped and un-trapped atoms after the application of single RF pulses of varying amplitude; it was critical to establish agreement between experiment and theory in a simple mode of operation before pursuing studies of more complex dynamics. In Fig. 1, we show the results of these measurements in comparison with a one dimensional Gross-Pitaevskii theory of the atom laser derived from the full 3D model described by the following equations

$$\begin{aligned}
 i_{-2} &= (L + V_T + G y^2) i_{-2} + 2 i_{-1} \\
 i_{-1} &= (L + \frac{1}{2} V_T + G y) i_{-1} + 2 i_{-2} + \frac{P}{6} i_{-0} \\
 i_{-0} &= (L + G y) i_{-0} + \frac{P}{6} i_{-1} + \frac{P}{6} i_{-1} \\
 i_{-1} &= (L - \frac{1}{2} V_T + G y +) i_{-1} + 2 i_{-2} + \frac{P}{6} i_{-0} \\
 i_{-2} &= (L - V_T + G y + 2) i_{-2} + 2 i_{-1};
 \end{aligned} \tag{1}$$

where i_i is the GP function for the i th Zeeman state. $V_T = \frac{1}{2}(\kappa^2 + y^2) + z^2$; $L = \frac{1}{2}r^2 + U(\frac{1}{2}i_{-2}j_{-2})$. Here $\kappa = \omega_x = \omega_y = 12:65$ is the ratio of trapping frequencies, and ω_z are respectively the detuning of the RF field from resonance and the Rabi frequency, measured in units of $\omega_z = 2 \omega_z$. U is the two-body interaction coefficient and $G = z_0 m g = (\hbar \omega_z)$, where m is the atomic mass and g the acceleration due to gravity. $z_0 = \frac{\hbar}{m \omega_z}$ is the usual harmonic oscillator length. The wave func-

tions, time, spatial coordinates, and interaction strengths are measured in the units of z_0 , and ω_z^{-1} . The excellent agreement between experiment and theory shown in Fig. 1 indicates that we have a well calibrated and repeatable experiment. Up to the experimental uncertainty in the detuning, there are no free parameters in the 1D GP model. The theoretical results of the Rabi oscillations presented in Fig. 1 are in good agreement with the approximate analytic theory presented by Graham and Walls for the limit of strong out-coupling [19].

In the experimental data shown in Fig. 2, we present five pulse trains outcoupled from separate $F=2$, $m_F = 2$ condensates. In each case, the pulse train has been out-coupled in an 8 ms time frame. We wait 2 ms after the pulse window before turning the trap off to allow the atomic pulse to completely separate from the condensate. After a further 2 ms, to allow expansion of the condensate, we image the condensate and pulses with a single lens onto a 12 bit CCD camera. For one, two, three and four RF pulses, we observe predictable out-coupling from the atom laser system. Figure 2(a) is indicative of this behavior, where four RF pulses (separation 2 ms) have been applied to the BEC, and we see four $m_F = 0$ atomic pulses in the positions expected from gravity. In 2(b) five RF pulses (separation 1.6 ms) have been applied and we observe five atomic wave-packets, again in the expected positions. However, we note that in the later 3 pulses there is a significant blurring with atoms appearing between the expected positions of the pulses. This effect is not due to interference between the wavepackets.

The transition from constant pulse amplitude shown in Fig. 2(a) to varying or noisy pulse amplitude with increasing repetition rate shows a clear trade off between classical noise and flux in the atom laser output. In Fig. 2(c) six RF pulses were applied (separation 1.2 ms), however only five atomic pulses were observed, with the first atomic pulse being entirely absent. This observation is quite repeatable. The complete absence of a pulse is an extreme example of the trade off between classical noise and flux, and it is the dynamics behind this phenomenon that we wished to understand by comparison with a complete 3D GP model. At the higher pulse repetition rate used in Fig. 2(d) where the separation between pulses is 1 ms, the output is further distorted from the ideal. In Fig. 2(e), where the time between pulses has been reduced to 800 μ s, the atom laser beam is longer than expected from pure gravitational acceleration. This can be explained by the influence of the anti-trapped m_F states on the $m_F = 0$ atoms that comprise the outcoupled beam. It is quite clear from the data that increasing flux (and therefore decreasing shot noise) comes at the price of increasing classical noise.

We have quantitatively modelled the experiment with a full 3D GP simulation including all five Zeeman states and with only the detuning as a free parameter (Eq. 1). This is a unique feature of the work presented here and

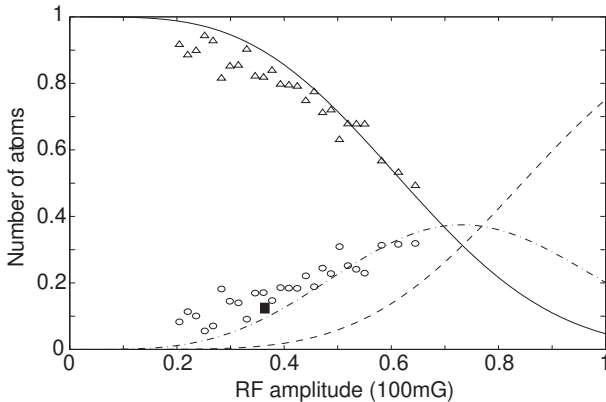


FIG. 1: Outcoupled fraction as a function of RF amplitude. The solid square is the power at which the results of Fig. 2 were generated. Theoretical curves are: Solid line, $m_F = 2; 1$ trapped states, dot-dashed $m_F = 0$ and dashed, $m_F = 2; 1$ anti-trapped states. The experimental results are: triangles, $m_F = 2; 1$ trapped states, circles $m_F = 0$. Typical error bars are 5% vertically and 10% horizontally. Simulation parameter: $\omega_z = 640$.

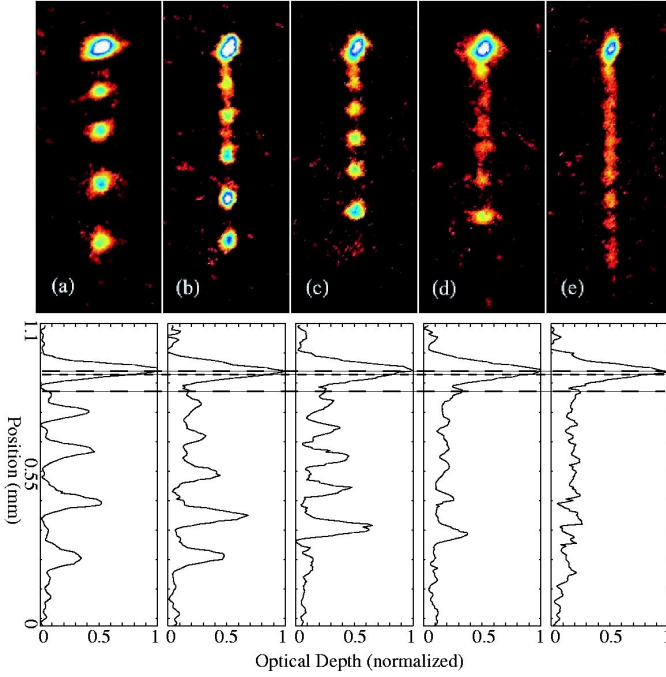


FIG. 2: (color) A series of pulsed atom lasers at different pulse rates. The applied radio-frequency (RF) pulses are varied from (a) 4 pulses, (b) 5 pulses, (c) 6 pulses, (d) 7 pulses, (e) 10 pulses in an 8 ms window. The lower plots show a cross-section down the centre of the absorption data. The three dashed lines correspond in descending order to the centre of the condensate, the half-width of the 200 kHz RF resonance (100 kHz \pm 12 m in our trap) and the position coinciding with the final RF out-coupling pulse (4 ms prior to imaging).

allows us to understand all aspects of the GP physics, and hence the experiment. A 1D model accurately describes a single out-coupling pulse because it is essentially independent of the spatial structure. However we found that a full 3D simulation was needed to accurately track the spatio-temporal dynamics of a multipulse experiment. We simulated up to 3.2 ms, allowing three pulses for each case. Parallelised code was run on twelve processors of the APAC National Facility [20], requiring up to 800 hours of processor time per simulation. The numerical method was the pseudo-spectral method with Runge-Kutta split time step developed at the University of Oxford [21]. Spatial grid sizes and time steps were monitored throughout the simulations to ensure the accuracy of the numerical solutions; e.g. the preservation of the normalisation. Spatial grids were grown, and time steps decreased, as required. At the end of simulations, spatial grids in the direction of gravity were 2048 points for the trapped ($m_F = 2; 1$) and anti-trapped ($m_F = 2; 1$) Zeeman states, and 4096 for the atom laser output state ($m_F = 0$). In the tight and loose transverse directions, 128 and 32 points were used respectively. The corresponding spatial lengths were chosen so that both the momentum space and real space GP functions fit the

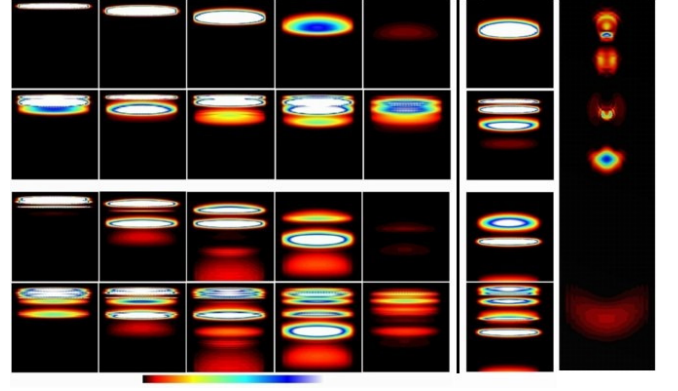


FIG. 3: (color) Numerical simulations of the cases of Fig. 2(c) and 2(b). Case 2(c) is to the left of vertical line. Each image shows the GP wavefunction density, in arbitrary units, integrated through the tight trap direction. Density is indicated by the color bar at the bottom of the figure, with black and white corresponding to zero and high density respectively. Each image is 120 μ m in both directions. From top to bottom the rows are: $t = 1.2$ ms, just before the 2nd RF pulse; just after the 2nd RF pulse; $t = 2.4$ ms, just before the 3rd RF pulse; just after the 3rd RF pulse. $t = 0$ is the beginning of the first RF pulse. The columns from left to right are the $m_F = 2; 1; 0; 1; 2$ states. The top-left image therefore shows the trapped position of the initial $m_F = 2$ condensate. Case 2(b) is to the right of vertical line. Only the $m_F = 0$ state is shown. The rows are as before but the RF pulses occur at $t = 1.6$ ms and $t = 3.2$ ms. Each image is 120 μ m vertically and 140 μ m horizontally. The rightmost image shows the $m_F = 0$ state density on a slice plane through the tight trap direction, just after the 3rd RF pulse. It is 40 μ m horizontally and about 150 μ m vertically, allowing the first pulse to be seen. Simulation parameters: $\hbar = 633$, $\mu = 457$. See text for discussion.

grid. This was about 40 μ m and 140 μ m in the tight and loose trap directions, respectively. In the direction of gravity, it was 120 μ m for the $m_F \neq 0$ states, and twice that for the $m_F = 0$ state. Absorbing boundaries were used for the $m_F = 0; 1; 2$ states.

The simulations reveal that all five Zeeman states are involved in determining the final form of the atom laser output. The $m_F = -2$ state has the least effect, as it is not strongly populated, and it quickly disperses in its anti-trapping potential. However the $m_F = -1$ anti-trapped state is highly populated and is directly involved in the loss of the initial pulse for the case of Fig. 2(c). The simulation in the left section of Fig. 3 shows how the first $m_F = 0$ atom laser pulse is destroyed by the second RF pulse: it transfers nearly all of the $m_F = 0$ component, produced by the first pulse, into the other four Zeeman states (second row, Fig. 3). A new $m_F = 0$ pulse, somewhat lower than the first, originates from the $m_F = -1$ state. However, it retains the momentum spread due to the anti-trapping potential, which causes it to disperse and be lost, so that it is not observed in the experiment.

The second atom laser pulse is in fact two distinct pulses; an upper one originating from the $m_F = 2$ state, and a lower one from the $m_F = 1$ state. This can be seen most clearly in the third row of Fig. 3, after they have become well separated. Since the two pulse components are not resolvable in the experiment, this is an example of the dynamics revealed by simulation. These components have different initial momenta. The $m_F = 1$ component, which originated from the $m_F = 2$ state in the first RF pulse, was moving down towards its trap equilibrium when the second RF pulse arrived.

The lower $m_F = 0$ pulse created by the second RF pulse escapes the fate of the first pulse because its downward momentum takes it lower than the first pulse, away from resonance. In fact, its position is close to that of the upper second $m_F = 0$ pulse during the third RF pulse in the case of Fig. 2(b), and it survives for similar reasons. This can be seen by comparing the bottom rows of the $m_F = 0$ columns of Fig. 3. Similarly the simulations explain the relative intensity of the first and second $m_F = 0$ pulses in the experimental case of Fig. 2(b).

We have shown, for the case of the $F = 2$ atom laser, that beyond a critical flux the classical noise on the output beam increases with increasing flux. The prospect of combining atom lasers with atom chips opens up enormous possibilities in precision measurement. Considerations of the trade off between classical noise and flux in atom lasers will be important in many applications in this field. We would expect many of the effects described here to be smaller for the $F = 1$ atom laser but not absent. Rather than the two trapped states present in the $F = 2$ laser, only the $m_F = 1$ state is trapped. Although atoms in the $m_F = 1$ state are anti-trapped for the $F = 1$ laser, this state would be significantly populated for strong outcoupling and could be expected to contribute to classical noise on the $m_F = 0$ output beam just as the anti-trapped $m_F = 1$ state does for the $F = 2$ laser studied in this Letter. The effects that we have described will be important not only for pulsed atom lasers, but also for unpumped continuous atom lasers. Just as in the pulsed case, at high flux, atoms will not only be coupled to the output beam, they will also be coupled to other trapped and untrapped Zeeman states and can be backcoupled from the output beam to the condensate. The situation is complex and requires detailed investigation. The quantitative comparison between the-

ory and experiment presented here is unique and points the way to the future development of atom laser sources for precision measurement. This is particularly true for the development of the pumped atom laser, one of the most important and sought-after devices in the field of atom optics.

This research was supported by the Australian Partnership for Advanced Computing. ACQAO is an Australian Research Council Centre of Excellence.

Electronic address: nick.robins@anu.edu.au; URL: <http://www.acqao.org/>

- [1] S. L. Rolston and W. D. Phillips, Nature 416, 219 (2002).
- [2] W. Ketterle, Physics Today, 52, 30, (1999).
- [3] T. L. Gustavson, P. Bouyer, and M. A. Kasevich, Phys. Rev. Lett. 78, 2046 (1997).
- [4] S. A. Haine et al., Phys. Rev. Lett. 88, 170403 (2002).
- [5] M. O. Mewes et al., Phys. Rev. Lett. 78, 582 (1997).
- [6] E. W. Hagley et al., Science 283, 1706 (1999).
- [7] I. Bloch et al., Phys. Rev. Lett. 82, 3008 (1999).
- [8] I. Bloch et al., Phys. Rev. Lett. 87, 030401 (2001).
- [9] M. Kohl, T. W. Hansch, T. Esslinger, Phys. Rev. Lett. 87, 160404 (2001).
- [10] I. Bloch, T. W. Hansch, T. Esslinger, Nature 403, 166, (2000).
- [11] B. P. Anderson and M. A. Kasevich, Science 282, 1686 (1998).
- [12] Y. Le Coq et al., Phys. Rev. Lett. 87, 170403 (2001).
- [13] M. Kohl, T. W. Hansch, T. Esslinger, Phys. Rev. A 65, 021606, (2002).
- [14] R. J. Ballagh, K. Burnett, and T. F. Scott, Phys. Rev. Lett. 78, 1607 (1997);
- [15] J. Schneider and A. Schenzle, Appl. Phys. B 69, 353 (1999).
- [16] H. Steck, M. Naraschewski, and H. Wallis, Phys. Rev. Lett., 80, 1 (1998).
- [17] M. W. Jack, M. Naraschewski, M. J. Collett and D. F. Walls, Phys. Rev. A 59, 2962 (1999).
- [18] G. M. Moly, J. J. Hope, and C. M. Savage, Phys. Rev. A 59, 667 (1999).
- [19] T. Esslinger et al., Phys. Rev. A 58, 2664 (1998).
- [20] R. Graham and D. F. Walls, Phys. Rev. A 60, 1429 (1999).
- [21] Australian Partnership for Advanced Computing National Facility: <http://nfapac.edu.au/>
- [22] B. M. Caradoc-Davies, Ph.D. Thesis, Univ. of Otago: <http://www.physics.otago.ac.nz/bec2/bmcd/>